Journal of Applied Fluid Mechanics, Vol. 18, No. 9, pp. 2389-2405, 2025.
Available online at www.jafmonline.net, ISSN 1735-3572, EISSN 1735-3645.
https://doi.org/10.47176/jafm.18.9.3224

Turbulence and Combustion Model Choice for Modeling Methane-air Low Swirl Burners

M. Ladjani, M. S. Lounici and S. Ouchikh †

Energy, Mechanics & Engineering Laboratory (LEMI), Faculty of Technology, M'hamed Bougara University of Boumerdes, Independence Avenue 35000 Boumerdes, Algeria

†*Corresponding Author Email: s.ouchikh@univ-boumerdes.dz*

ABSTRACT

Combustion plays a major role in satisfying enormous needs in our world, and burners are an essential component of industrial combustion applications. With its flame stabilization technique, low swirl burner (LSB) technology offers interesting outcomes in reducing pollutant emissions and preserving industrial facilities. Numerical simulation provides a valuable contribution to the development of such systems. However, the relevance of the simulation depends on the different models used. The present study aims to investigate two combustion models (Eddy Dissipation and Partially-Premixed) coupled with various Reynolds-averaged Navier-Stokes (RANS) turbulence models to identify the most appropriate models for LSBs. Thus, simulation results were compared to experimental data available in the literature for various LSB burners. The influence of turbulence and combustion model choice was found to be considerable. Specifically, coupling the RANS RNG k-ε turbulence model with the Partially-Premixed combustion model to simulate reactive flow in such burners offers very satisfactory outcomes.

Article History

Received October 26, 2024
Revised April 21, 2025
Accepted April 24, 2025
Available online July 5, 2025

Keywords:

Combustion models
Eddy dissipation model
Low swirl burner
Partially premixed model
Reynolds-averaged Navier-Stokes turbulence models

1. INTRODUCTION

Nowadays, combustion is a significant factor required to meet the vast demands of our global society. In industrial combustion applications, as burners represent essential components, an appropriate comprehension of these applications is essential for selecting the appropriate burner type (Borghi & Destriau, 1995). However, burners are one of the largest environmental polluters. Fortunately, their emissions can be reduced in some cases by combustion techniques, including lean burn combined with flame stabilization adaptations. Dry-Low NOx (nitrogen oxide) technology appears to be a solution for cleaner combustion with reduced NOx and CO (carbon monoxide) emissions (Abdulnaim et al., 2024; Carlsson et al., 2014). Such burners must operate near the lean-blow limit (LBO) where noise, instability, and flame blow-off can seriously affect performance and reliability (Cheng et al., 2009; Gong et al., 2023).

Low swirl burners (LSBs) offer a promising method of flame stabilization. Their uses are vast and beneficial, including internal combustion engines, gas turbines combustion chambers, industrial furnaces, and boilers (Al-Abdeli & Masri, 2015; Chong et al., 2016). The concept of flame stabilization by LSB technology was introduced by Chan et al. (1992), who conducted experimental studies for the characterization of premixed flames by injecting a small amount of air tangentially into the co-flow of a concentric burner (swirl number between 0.05 and 0.3). Bedat and Cheng (1995) conducted a follow-up study (Fig. 1). Those studies yielded promising results, encouraging many research groups to carry out additional experimental investigations on this technique of flame stabilization and polluting emissions reduction. In addition, other numerical studies have been carried out to better understand and characterize this type of flame.

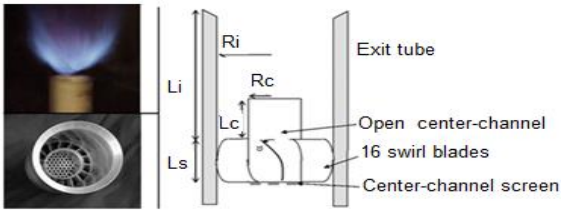

Fig. 1 LSB burner elaborated by Bedat and Cheng (1995)

As swirling flow is complex and chaotic, the careful selection of a turbulence model is necessary for reliable

NOMENCLATURE

C	reaction progress variable	I	turbulence intensity
D_h	hydraulic diameter	Ω	swirl number
U_c	axial velocity of the perforated plate	U_{st}	tangential velocity of the swirled space
U_0	average entry speed	U_s	axial velocity of the swirled space
Sc_t	turbulent Schmidt number	υ_i'	stoichiometric coefficients for reactant i
$Y_{\mathcal{R}}$	mass fraction of a specific reactant $\mathcal{R}$	υ_j''	stoichiometric coefficients for product j
M_w	molecular mass of a species	Y_P	mass fraction of any product P
u'	RMS (root-mean-square) velocity	U_l	laminar flame speed
α	unburnt thermal diffusivity	l_t	turbulence length scale

numerical simulations. To examine the impact of the turbulence model, Fudihara et al. (2003) investigated the aerodynamics of a movable block swirl burner, which is distinguished by its capacity to continuously and dynamically modulate the swirl intensity through the simultaneous rotation of eight movable blocks positioned between eight fixed blocks. Two k-ε turbulence models, specifically the RNG k-ε (renormalization group) and STD k-ε (standard), were utilized. The researchers determined that only the RNG k-ε model accurately represented the presence of a center reverse flow within the annular area and yielded results more aligned with the experimental data from the International Flame Research Foundation (IFRF).

Li and Jia (2014) examined the effect of swirl on the formation of polluting emissions and the characteristics of methane flames at high air temperatures with swirling and non-swirling configurations. In their numerical simulation, they employed the Speziale-Sarkar-Gatski (SSG) Reynolds stress turbulence model with the Eddy Dissipation Model (EDM) for combustion. They found that the flame with swirling flow creates a stable temperature distribution. However, flame with non-swirling shows a different temperature distribution and thermal-NO formation is much higher than swirling case.

Tidswell et al. (2018) employed various RANS (Reynolds-averaged Navier-Stokes) turbulence models, namely RNG k-ε, RZ k-ε (Realizable), STD k-ω, and SST k-ω (Shear Stress Transport) coupled with the premixed combustion model. This study was conducted to establish the most effective turbulence model for a low-swirl hydrogen-methane-air flame, with 0 to 100% hydrogen. As a result of this investigation, k-ε RZ with the Zimont model was found to be the optimal choice for up to 60% hydrogen. In another numerical work, Muppala et al. (2015) compared five turbulent combustion models namely Linstedt-Vaos (LV), Bray-Moss-Libby (BML), Turbulent Flame speed Closure (TFC), a modified LV version, and Algebraic Flame Surface Wrinkling (AFSW)) with the RNG k-ε turbulence model for a LSB with pure methane-air, and 40 to 100 % hydrogen blends. They demonstrated the significance of preferential diffusion and Lewis number effects on predictions of hydrogen-enriched hydrocarbon flames. Furthermore, the AFSW model's predictions for pure methane flames coincided well with experimental results.

To study the effect of equivalence ratio and swirl number, Ouali et al. (2016) used a numerical simulation of a premixed methane-air LSB burner in two configurations (two- (2D) and three-dimensional (3D)). They used the RANS STD k-ε model for turbulence coupled with the Eddy Dissipation model and the Partially Premixed model (PPC) to treat combustion. Their results were compared to experimental and Large Eddy Simulation (LES) results available in the literature.

Cellek et al. (2018) investigated LSB burner performance and emission characteristics during combustion of pure and hydrogen-enriched natural gas, using ANSYS Fluent. They demonstrated that using Eddy dissipation combustion model with a methane-air-2step reaction combined with the RZ k-ε turbulence model for moderate swirl flows shows good agreement with experimental results.

Pang et al. (2018) conducted a comparative study modeling the combustion of a natural gas swirl burner with the 2-step finite rate/eddy dissipation (FR/EDM) and the PPC model, coupled with a detailed chemical mechanism and STD k-ε, RZ k-ε, and RNG k-ε turbulence models. 325 reactions and 53 species were employed. Additionally, Discrete Ordinates (DO) and spherical harmonics (P1) models were applied for predicting thermal radiation. They found that integrating multi-step chemistry into the partially premixed model along with STD k-ε and P1 models yields accurate predictions, with an average variance of approximately 7.8% for combustion temperature and 15.5% for chemical species concentration.

Pashchenko (2020) performed a Computational Fluid Dynamics (CFD) simulation with experimental verification of swirled methane lean mixture flames enriched with hydrogen. The premixed combustion model coupled with the RNG k-ε turbulence model were used. The deviation of CFD results from experimental measurements was about 3% for temperature and less than 7% for NOx emissions. Stefanizzi et al. (2021) investigated numerically, using ANSYS Fluent, swirled premixed burner, both in the case of cold and hot flow. Pure methane and a 30%H_2 blend were employed. A 3D unsteady RANS approach was used. Partially premixed combustion model and Reynolds stress model (RSM) were implemented. The results were validated using experimental data. Results showed that, by introducing hydrogen in the fuel mixture, carbon dioxide production is reduced by approximately 10%.

Bouziane et al. (2021) studied a premixed CH_4-H_2-air LSB burner using 2D ANSYS Fluent simulation. They employed STD k-ε and RNG k-ε models for turbulence and the finite rate/eddy dissipation (FR/ED) concept for

combustion. The fuel stream's hydrogen concentration varied from 0% to 100%, and outcomes demonstrated that the RNG k-ε model can accurately predict the flame shape and corresponds well with experimental data. Xiao et al. (2022) simulated steady turbulent combustion of methane in a confined 2D LSB with a PPC model. The research investigated the effects of swirl angle (θ=35°-47°), equivalence ratio (ϕ=0.6-0.9), and axial flow radius (R=0.6-0.7) on temperature distribution, flame length, flame rise length, velocity field, streamlines, and pollutant species. Experimental measurements were used to validate the simulation, with results showing that the maximum temperature of the flame moves closer to the reactant inlet and the strength of the axial flow decreases as the fuel-to-air ratio increases. Also, by increasing the swirl angle, the position of the minimum velocity value tends towards the outlet and the maximum temperature of the combustion chamber increases.

Nemitallah et al. (2023) investigated the 2D combustion characteristics and behavior of premixed oxy-flames in various methane-hydrogen mixtures using numerical simulations in a dual annular counter-rotating swirl (DACRS) combustor. The study employed the STD k-ε model for turbulence and the PPC model, combined with the Zimont model for turbulent flame speed. Radiative heat transfer was considered using Discrete Ordinates (DO) modeling. Hydrogen fraction mixtures ranging from 25% to 100% were examined. The results showed that as the hydrogen fraction increases, the inner recirculation zone shrinks and eventually disappears, leaving only the outer recirculation zone at 100% hydrogen fraction. Stable well-anchored flames were achieved over the examined fuel mixtures. Daurer et al. (2024) studied experimentally and numerically the combustion characteristics of hydrogen enrichment in natural gas (NG) from 0 to 100 vol% within a low-swirl burner inside a combustion chamber using 3D RANS. They employed the Standard and Realizable k–ε models for turbulence and the PPC Model with Steady Laminar Flamelet (SLF). Thermal radiation was considered. An increase in the process efficiency and a reduction in NOx emissions were observed for hydrogen-enriched combustion.

Mazzotta et al. (2025) conducted a 3D comparative analysis of several turbulence models, including Large Eddy Simulation (LES), RZ and RNG k-ε, SST k-ω, and the Reynolds Stress Model (RSM) to simulate the premixed swirl combustion of ammonia/hydrogen mixtures. The Flamelet Generated Manifold (FGM) method was used with a detailed chemistry scheme. The main objective of the study was to identify the most suitable turbulence models for this application. Overall, among the RANS models, the RSM model provided results closest to those of the high-fidelity LES.

The objective behind the present study is to develop a reliable, low-cost simulation tool that can serve for LSB development. Different approaches are adopted in the literature. Because time and resource costs associated with Direct Numerical Simulation and LES approaches are significant, the RANS approach has been established as a key method in the industrial sector due to its low

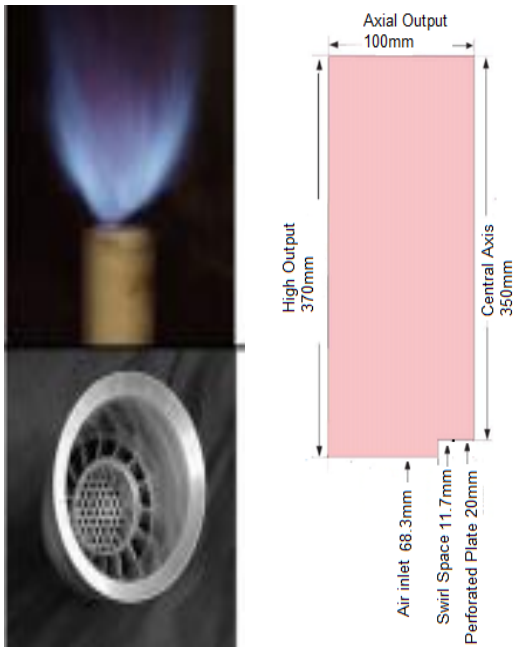

(a) (b)

Fig. 2 (a) photo, (b) geometry of the computational domain corresponding to the LSB of Littlejohn and Cheng (2007)

computational cost and high reliability (Nanduri et al., 2010). Several RANS models are used for LSB burners in the literature, but in general, no choice influence is investigated. Therefore, the present study aimed to study the influence of turbulence and combustion model choice and recommend the most appropriate of these.

Thus, various RANS turbulence models (STD k-ε, RNG k-ε, RZ k-ε, STD k-ω, and SST k-ω) coupled with two combustion models (EDM and PPC), widely used in previously published works and less costly, are investigated for such burners. Simulation results are compared to experimental data available in the literature for various LSB burners.

The present investigation used different LSB burners to obtain more general conclusions. Namely, the numerical simulation was carried out for two atmospheric pressure low swirl burners (LSB ATP) and a third LSB burner inside a combustion chamber (LSB CC).

2. PROBLEM MODELING

CFD simulation outcomes for various LSBs were compared to experimental data available in the literature. The simulations were carried out using ANSYS Fluent 16.

A 2D axisymmetric swirl model is adopted for the three flame configurations. The geometry was realized using Gambit. Half of the geometry is introduced.

Figure 2 (a) shows a photo and (b) the adopted geometry for the low swirl burner 1 under atmospheric pressure (LSB1 ATP), used in the study of Littlejohn and Cheng (2007).

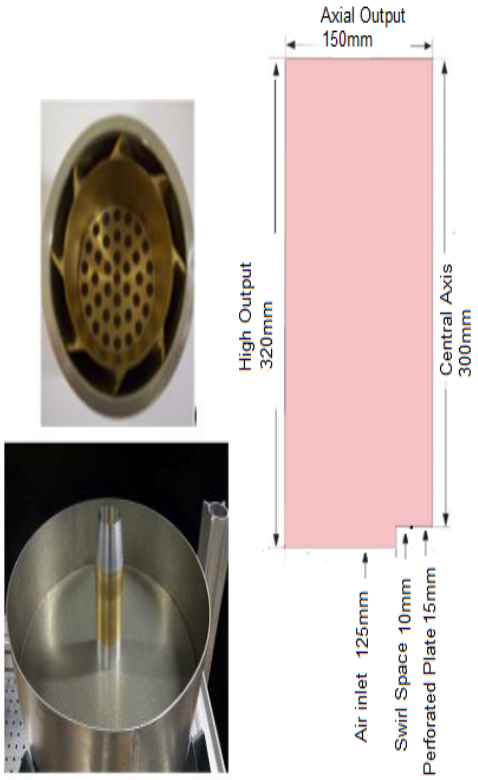

(a) (b)

Fig. 3 (a) photo, (b) geometry of the computational domain corresponding to the LSB of Nogenmyr et al. (2009)

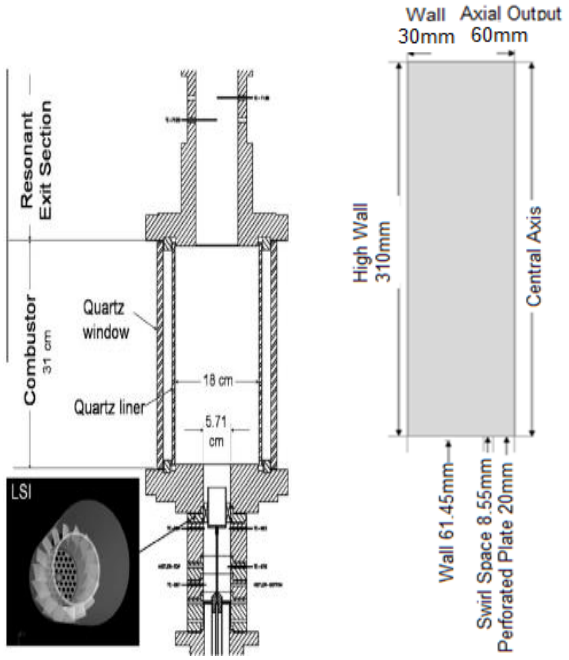

(a) (b)

Fig. 4 (a) photo, (b) geometry of the computational domain corresponding to the LSB of Cheng et al. (2009)

The burner nozzle has a radius of 31.7 mm. It consists of two parts: the axial perforated plate where the reactive mixture is injected with purely axial velocity in a radius of 20 mm, and a swirled annular space of 11.7 mm where the reactive mixture is injected with two speed components (axial and tangential). It does not have solid walls; the whole field of calculations is open to the atmosphere. As in the numerical study of Nogenmyr et al. (2009), the air inlet is shifted rearwards by 20 mm. Both reactive flow (RF) and non-reactive flow (NRF) cases were considered.

Figure 3 (a) displays a photo and (b) the adopted geometry for the low swirl burner 2 under atmospheric pressure (LSB2 ATP) used in the study of Nogenmyr et al. (2009).

The burner nozzle has a radius of 25 mm. It consists of two parts: the axial perforated plate where the reactive mixture is injected with purely axial velocity in a radius of 15 mm, and a swirled annular space of 10 mm where the reactive mixture is injected with two speed components (axial and tangential).

Figure 4 represents the low swirl burner 3 in a combustion chamber (LSB3 CC), which consists of the LSB burner inside a combustion chamber used in the study of Cheng et al. (2009). Figure 4 (a) shows a photo of the burner and dimensions of the combustion chamber. Figure 4 (b) displays the adopted geometry for the simulation.

The burner nozzle has a radius of 28.55 mm. It consists of two parts: the axial perforated plate where the reactive mixture is injected with purely axial velocity in a radius of 20 mm, and a swirled annular space of 8.55 mm, where the reactive mixture is injected with two speed components (axial and tangential).

2.1 Governing Equations

The governing phenomenon is reactive flow (RF). The density of the species is calculated using the incompressible ideal gas assumption at burner inlets given that the Mach number is less than 0.3 (Anderson Jr, 1991). Conservation equations for mass, momentum, energy, and chemical species govern the flow and heat transfer of the incompressible Newtonian fluid (methane-air) in the current study. The flow physics is described by using the steady-state, Reynolds-averaged Navier-Stokes equations for mass, momentum, energy and chemical species. The reactive flow is described using a 2D axisymmetric swirl approach. Because the 3D geometry in the case of LSBs is symmetrical about its axis, the azimuthal variations can be neglected. Therefore, it is still sufficient to limit the simulations to axisymmetric 2D domains, thus saving significant amounts of computational time and effort (Fluent, 2015; Xiao et al., 2022). Radiation has not been taken into consideration. The findings of many investigations (Ouali et al., 2016; Bouziane et al., 2021; Xiao et al., 2022) confirmed this approach.

- *Continuity equation*

$$\frac{\partial}{\partial x_j}\left(\rho u_j\right) = 0 \tag{1}$$

Where ρ is the density of the fluid and u_j is the velocity component in the j-direction.

- *Momentum equation*

$$\frac{\partial}{\partial x_j}(\rho u_i u_j) = -\frac{\partial p}{\partial x_j} + \frac{\partial \tau_{ij}}{\partial x_j} + \frac{\partial}{\partial x_j}(-\rho\overline{u_i' u_j'}) + F_j \quad (2)$$

Where τ_{ij} is the viscous tensor, and $-\rho\overline{u_i' u_j'}$ is the component of the tensor of Reynolds stress given by

$$\tau_{ij} = \mu\left[\left(\frac{\partial u_i}{\partial x_j} + \frac{\partial u_j}{\partial x_i}\right) - \frac{2}{3}\delta_{ij}\left(\frac{\partial u_i}{\partial x_j}\right)\right] - \rho\overline{u_i' u_j'} = \mu_t\left(\frac{\partial u_i}{\partial x_j} + \frac{\partial u_j}{\partial x_i}\right) - \frac{3}{2}\delta_{ij}\left(\rho k + \mu_t \frac{\partial u_i}{\partial x_j}\right) \quad (3)$$

Where p is the pressure, μ_t is the turbulent viscosity, and μ is the dynamic viscosity. F_j is the volume force of gravity.

Where

$$\mu_t = \rho C_\mu \frac{k^2}{\varepsilon} \quad (4)$$

- *Energy equation*

It is the equation most affected by combustion dynamics. It can be written in several forms, one of the most used of which is that of sensible enthalpy:

$$\frac{\partial}{\partial x_j}(\rho u_j h) = \frac{\partial}{\partial x_j}\left(\rho D_h \frac{\partial h}{\partial x_j} - \rho\ \overline{h' u_j'}\ \right) \quad (5)$$

where $D_h = \frac{\lambda}{\rho c_p}$ is the thermal diffusivity, h is the specific enthalpy defined by the mass enthalpy for each species.

- *Chemical species equation*

$$\frac{\partial(\rho u_i Y_k)}{\partial x_j} = -\frac{\partial J_j^k}{\partial x_i} + \rho \dot{W}_k \quad (6)$$

where Y_k is the mass fraction, and J_j^k is the diffusive mass flux of species k in the j direction.

$$J_j^k = \rho u_j^k Y_k \quad (7)$$

where u_k^j is the i^{th} component of the diffusion velocity of species k, and $\dot{W}_k$ is the production rate of the species k. The reaction rate is the sum of the reaction rates $W_{k,j}$ of the M reactions:

$$\dot{W}_k = \sum_{j=1}^{M} \dot{W}_{k,J} \quad (8)$$

2.2 Turbulence Modeling

The RANS method is employed for the resolution of turbulent flow phenomena. Various models, including STD k-ε, RNG k-ε, k-ε RZ, STD k-ω, and SST k-ω, were examined. The RANS k-ε and k-ω models utilize transport equations that describe turbulence kinetic energy (k) and dissipation rate (ε) or turbulent frequency (ω), respectively.

The STD k-ε model is the simplest model in which two equations define turbulence.

The transport equation for the dissipation rate in the STD k-ε model is represented in Eq.9.

$$\frac{\partial}{\partial x_i}(\rho\varepsilon u_i) = \frac{\partial}{\partial x_j}\left[\left(\mu + \frac{\mu_t}{\sigma_\varepsilon}\right)\frac{\partial \varepsilon}{\partial x_j}\right] + C_{1\varepsilon}\frac{\varepsilon}{k}(G_k + C_{3\varepsilon} G_b) - C_{2\varepsilon}\rho\frac{\varepsilon^2}{k} + S_\varepsilon \quad (9)$$

The model constants are: C_μ=0.09, $\sigma_\varepsilon = 1$, $C_{1\varepsilon} = 1.44$, and $C_{2\varepsilon} = 1.92$,and $\sigma_k = 1$.

The turbulent kinetic energy equation for k-ε STD is modeled in Eq.10.

$$\frac{\partial}{\partial x_i}(\rho k u_i) = \frac{\partial}{\partial x_j}\left[\left(\mu + \frac{\mu_t}{\sigma_k}\right)\frac{\partial k}{\partial x_j}\right] + G_k + G_b - \rho\varepsilon - Y_M + S_k \quad (10)$$

where k represents turbulent kinetic energy, while $G_k$and G_b indicate the production rates attributed to the mean velocity gradient and buoyancy, respectively. The ε indicates the dissipation rate, and Y_M refers to the dilatation dissipation term that accounts for the effects of compressibility. $S_k$and S_ε are source terms.

The turbulent viscosity,μ_t, is calculated by combining the variables k and ε as follows:

$$\mu_t = \rho C_\mu \frac{k^2}{\varepsilon} \quad (11)$$

C_μ is a constant

The RZ k-ε model is another variant derived from the STD k-ε model. It is distinct from the STD k-ε model due to its variable turbulent viscosity. The turbulent viscosity coefficient $C_\mu$is calculated based on the local flow states to guarantee a positive normal stress $\overline{u_i' u_j'}$ for all flow conditions.

C_μ for the RZ k-ε model is computed by Eq.12 (Fluent, 2015; Pang et al.,2018):

$$C_\mu = \frac{1}{A_0 + A_s\frac{kU^*}{\varepsilon}} \quad (12)$$

Where

$A_0 = 4.04$, $A_s = \sqrt{6}\cos\varphi$, $\varphi = \left(\cos^{-1}\left(\sqrt{6}w\right)/3\right)$,

$w = \left(S_{ij}S_{jk}S_{ki}/\widehat{S_3}\right)$ and $\widehat{S_3} = S_{ij}S_{ij}$.

$$with\ S_{ij} = \frac{1}{2}\left(\frac{\partial u_i}{\partial x_j} + \frac{\partial u_j}{\partial x_i}\right)$$

$$and\ U^* = \sqrt{S_{ij}S_{ij} + \widehat{\Omega_{ij}}\,\widehat{\Omega_{ij}}}$$

$with\ \widehat{\Omega_{ij}}$ is the mean rate-of-rotation tensor viewed in a rotating reference frame with the angular velocity.

The transport equation of dissipation rate in the k-ε RZ model is modeled using Eq.13:

$$\frac{\partial}{\partial x_i}(\rho\varepsilon u_i) = \frac{\partial}{\partial x_i}\left[\left(\mu + \frac{\mu_t}{\sigma_\varepsilon}\right)\frac{\partial \varepsilon}{\partial x_i}\right] + \rho C_1 - \rho C_2\frac{\varepsilon^2}{k+\sqrt{v\varepsilon}} + C_{1\varepsilon}\frac{\varepsilon}{k}C_{3\varepsilon}G_b \quad (13)$$

while the $C_{3\varepsilon}$ is computed using Eq.14.

$$C_{3\varepsilon} = tanh\left|\frac{v}{u}\right| \quad (14)$$

where v and u are the components of velocity parallel and perpendicular to the gravitational vector, respectively. The model constants are $\sigma_\varepsilon = 1.2$, $C_2 = 1.9$, and $C_{1\varepsilon} = 1.44$. The coefficient, C_1, is given by Eq.15:

$$C_1 = max\left[0.43, \frac{\eta}{\eta+5}\right] \quad (15)$$

with

$$\eta = S\frac{k}{\varepsilon}, S = \sqrt{2S_{ij}S_{ij}}$$

The RNG k-ε model incorporates several modifications compared with the STD k-ε model. It is generated from the instantaneous Navier-Stokes equations by a mathematical technique known as the "renormalization group" method.

The smaller-scale eddies are eliminated, and the transport coefficient is renormalized. An additional factor (R_ε) was added to the dissipation rate transfer equation to account for turbulent and mean shear interactions. R_ε reduces the dissipation rate, resulting in lower effective viscosity. The buoyancy effect (G_b) generation rate differs from the STD k-ε and RZ k-ε models (Fluent, 2015).

In general, turbulence is affected by mean flow swirl. The RNG k-ε model could account for swirl or rotation by adjusting turbulent viscosity, making it well suited for swirling flows.

The modification function is as follows:

$$\mu_t = \mu_{t0} f\left(\alpha_s, \Omega, \frac{k}{\varepsilon}\right) \tag{16}$$

where the turbulent viscosity μ_{t0} is determined without the swirl modification, Ω is the characteristic swirl number, and α_s is the swirl constant that varies based on whether the flow is swirl-dominated or slightly swirling. For axisymmetric swirling flows, this swirl adjustment always applies with α_s set to 0.07.

The swirl number Ω is defined by:

$$\Omega = (2/3)tan\theta\left[\frac{1-R^3}{1-R^2+\left(m^2\left(\frac{1}{R^2}-1\right)^2 R^2\right)}\right] \tag{17}$$

with:

$$m = \frac{m_c}{m_s} = \frac{\pi\, U_c\, {R_c}^2}{\pi\, U_s\, (R_i^2 - R_c^2)} \tag{18}$$

The variable R represents the ratio of the radius of the central duct to the radius of the nozzle burner. The variable m denotes the ratio of the mass flow rate through the central plate to the mass flow rate through the annular swirled space. θ represents the inclination angle of the swirler vanes.

Regarding k-ω models, they define turbulent viscosity in terms of turbulent kinetic energy and turbulent frequency as follows:

$$\mu_t = \rho\frac{k}{\omega} \tag{19}$$

$$\frac{\partial}{\partial x_i}(\rho k u_i) = \frac{\partial}{\partial x_j}\left[\Gamma_k \frac{\partial k}{\partial x_j}\right] + G_k - Y_k + S_k \tag{20}$$

$$\frac{\partial}{\partial x_i}(\rho \omega u_i) = \frac{\partial}{\partial x_j}\left[\Gamma_\omega \frac{\partial \omega}{\partial x_j}\right] + G_\omega - Y_\omega + S_\omega + D_\omega \tag{21}$$

G_k is the production of turbulence kinetic energy, and G_ω is the production of ω.$Y_k$and Y_ω represent the dissipation of k and ω due to turbulence.

D_ω is the cross-diffusion term, S_k and S_ω are source terms.

Γ_k and Γ_ω represent the effective diffusivity of turbulent kinetic energy and the specific dissipation rate, respectively, and are calculated using the following equations (Eq.22 and 23):

$$\Gamma_k = \mu + \frac{\mu_t}{\sigma_k} \tag{22}$$

$$\Gamma_\omega = \mu + \frac{\mu_t}{\sigma_\omega} \tag{23}$$

where the default model constants are $\sigma_k = 2.0$ $\sigma_\omega = 2.9$

The STD k-ω model is recommended for flows characterized by a high swirl number. It is indicated for scenarios with high Reynolds numbers, particularly in highly confined or near-wall flow conditions. The model exhibits limitations, including challenges in convergence and an extended solution time compared to other models. Additionally, the SST k-ω model is employed to simulate the intense turbulent swirling motion of the fluid.

2.3 Combustion Modeling

Combustion is a complicated process, usually coupled with turbulence. Model selection is crucial, given that it directly affects the simulation results.

In the present study, two combustion models widely used in previously published works and less costly, were selected and investigated: EDM and PPC.

The EDM is a commonly used approach to simulate combustion phenomena, particularly in turbulent flows. It is often favored in combustion simulations for turbulent, high-speed flows, particularly in situations involving large-scale eddies and turbulent mixing, where it provides a robust and simplified approach. This model is principally effective in analyzing the combustion of gases in various applications, including industrial burners, automotive engines, and other combustion systems.

The EDM assumes that chemical reaction occurs much faster than reactants mixing, which mainly depends on turbulence. Thus, the reaction rate will be determined assuming that turbulent mixing is the rate-limiting process. In the present work, the EDM (Li & Jia, 2014; Ouali et al., 2016; Cellek & Pınarbaşı, 2018;) was implemented for (CH_4-air).

The net production rate of species i resulting from reaction r, denoted as R_i, is determined by the smaller of the two subsequent expressions (Magnussen & Hjertager, 1977):

Based on the mass fraction of reactants:

$$R_{i,r} = v'_{i,r} M_{w,i} A \rho \frac{\varepsilon}{k} min\left(\frac{Y_{\mathcal{R}}}{v'_{\mathcal{R},r} \cdot M_{w,\mathcal{R}}}\right) \tag{24}$$

Based on the mass fraction of products:

$$R_{i,r} = v'_{i,r} M_{w,i} AB \rho \frac{\varepsilon}{k}\left(\frac{\sum_P Y_P}{\sum_{j'}^{N} \upsilon''_{j',r}\, M_{w,j}}\right) \tag{25}$$

with $A = 4$ and $B = 0.5$ representing the Magnussen constants for reactants and products, respectively.

Regarding the partially premixed model (Nogenmyr et al., 2009; Stefanizzi et al., 2021), it is often used to simulate combustion processes where both premixed and

Table 1 Boundary conditions for air inlet

	LSB1 ATP NRF	LSB1 ATP RF	LSB2 ATP RF
U_a (m/s)	0.35	0.35	0.35
I (%)	0.1	0.1	0.1
D_h(mm)	136.6	136.6	250
CH_4 Mass fraction (-)	0	0	0
O_2 Mass fraction (-)	0.23	0.23	0.23
N_2 Mass fraction (-)	0.77	0.77	0.77

Table 2 Boundary conditions imposed on the perforated plate.

	LSB1 ATP NRF	LSB1 ATP RF	LSB2 ATP RF	LSB3 CC RF
U_0 (m/s)	6.76	9.27	5.00	18.0
U_c(m/s)	5.44	3.7	1.78	10.8
I (%)	10	10	10	10
D_h(mm)	40	40	30	40
CH_4 Mass fraction (-)	0.0408	0.0408	0.0348	0.0332
O_2 Mass fraction (-)	0.2236	0.2236	0.22	0.2254
N_2 Mass fraction (-)	0.7756	0.7756	0.7452	0.7414

Table 3 Boundary conditions imposed on the annular swirled space

	LSB1 ATP NRF	LSB1 ATP RF	LSB2 ATP RF	LSB3 CC RF
U_0 (m/s)	6.76	9.27	5.00	18.00
U_s(m/s)	8.16	12.9	3.8	19.8
U_{st}(m/s)	7.34	11.68	2.85	16.6
I (%)	10	10	10	10
D_h(mm)	23.4	23.4	20	17.1
CH_4 Mass fraction (-)	0.0408	0.0408	0.0348	0.0332
O_2 Mass fraction (-)	0.2236	0.2236	0.2200	0.2254
N_2 Mass fraction (-)	0.7756	0.7756	0.7452	0.7414

non-premixed characteristics are present in the flow. This is common in many real-world combustion systems, such as gas turbines, engines, and industrial burners, where fuel and air may mix in varying degrees before ignition.

The PPC model is based on both non-premixed (mixture-fraction-based) and premixed (reaction progress variable-based) combustion models.

This model solves a transport equation for the mean reaction progress variable $\bar{c}$, as well as the mean mixture fraction $\overline{f}$, and the mixture fraction variance $\overline{f'^2}$. Chemical equilibrium, partially premixed models have been exploited for the calculation of the progress variable. It assumes that the premixed flame front is infinitely thin, with unburnt reactants ahead and burnt products behind the flame front. The composition of the burnt products can be modeled assuming chemical equilibrium.

The key to the premixed combustion model is the prediction of the turbulent flame speed, which was determined using the Zimont model. It is applicable only when the smallest turbulent eddies of the flow are less than the flame thickness and extend into the flame zone. The concept is relevant to systems where the flame brush width expands over time, as noted in most industrial combustors.

The calculation is predicated on a model for wrinkled and thickened flame fronts.

$$U_t = A(u')^{3/4}(U_l)^{1/2}\alpha^{-1/4}{l_t}^{1/4} \quad (26)$$

where A is a model constant equal to 0.52.

The turbulence length scale l_t, is computed as:

$$l_t = C_D \frac{(u')^3}{\varepsilon} \quad (27)$$

with $C_D = 0.37$

2.4 Boundary Conditions

Boundary conditions for the computational domain were defined according to the data of the experimental studies considered, for which details are given in Section 2. They are summarized in Tables 1, 2, and 3.

2.5 Operating Conditions and Numerical Schemes

The operating conditions and dimensionless numbers adopted in this study are summarized in Table 4.

The equations of continuity, momentum, energy, and turbulent quantities are converted into algebraic equations using the finite-volume method on structured grids. The results were derived by resolving the incompressible Navier-Stokes equations using a pressure-based solver, 2D axisymmetric swirl, while gravitation forces have been neglected.

Table 4 Operating conditions and dimensionless numbers.

Parameter	LSB1 ATP	LSB2 ATP	LSB3 CC
Operating pressure	1 ATM	1 ATM	1 ATM
Inlet temperature	298 K	300 K	298 K
Reynolds number	27802	11400	64237.5
Equivalence ratio (ϕ)	0.73	0.6	0.59
Swirl number (S)	0.57	0.5	0.5
PDF Schmidt number	0.85	0.85	0.85
Number of Prandtl	0.85	0.85	0.85

Table 5 Numerical scheme

Case	RANS
Solver	Pressure-based, Steady axisymmetric swirl
Pressure-velocity coupling	SIMPLE
Pressure scheme	PRESTO
Momentum scheme	Second order upwind
Energy scheme	Second order upwind
Turbulence scheme	Second order upwind

For pressure-velocity coupling, the Semi-Implicit Method for Pressure-Linked Equations (SIMPLE) (Muppala et al., 2015; Rahman, et al. 2019; Bouziane et al., 2021) scheme was chosen. Presto was used for pressure discretization.

The calculation was regarded as converged when the scaled residual of the energy equation dropped to less than 1×10^{-8} and the other equations to be equal to 1×10^{-6}.

Table 5 illustrates the spatial discretization.

2.5 Meshing sensitivity

It is well known that CFD simulation results depend on the grid refinement. Therefore, it is necessary to determine the number of nodes ensuring the independence of the results with respect to the mesh. Moreover, this should provide an optimal compromise between accuracy of results and computational time.

To ensure the reliability of our results, a systematic analysis of grid independence and numerical scheme consistency was achieved. The grid independence study was performed by generating multiple meshes with different levels of refinement and comparing the results of a key variable across these meshes. The axial velocity and temperature variations according to node number were examined. Several simulations were carried out, as shown in Figs. 5,6, and 7. If the changes between successive mesh refinements become negligible, the results were considered grid-independent. The optimal mesh was selected by choosing the smallest mesh that provides accurate results to balance computational cost and accuracy.

To satisfy the above-mentioned criteria, a mesh with 36360 nodes for LSB1 ATP, 39901 for LSB2 ATP, and 27900 nodes for LSB3 CC was selected as the appropriate computational grid.

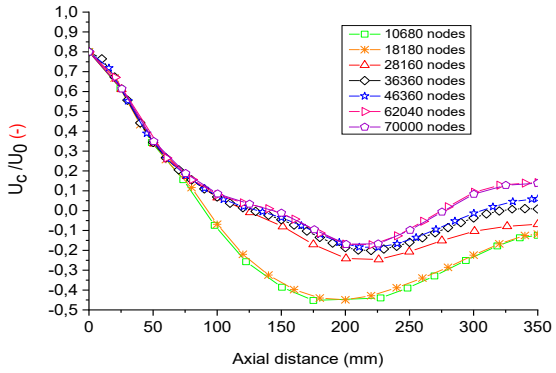

Fig. 5 Velocity ratio profiles along the LSB1 ATP axis for different meshes

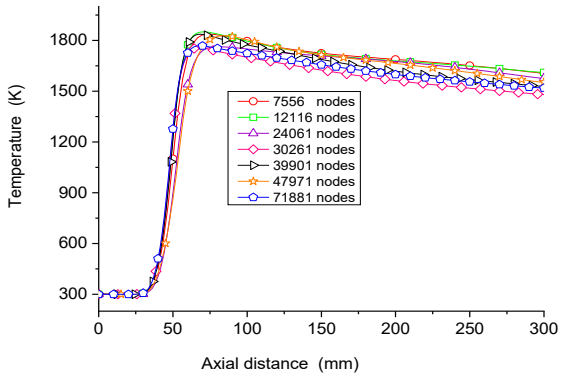

Fig. 6 Temperature profiles along the LSB2 ATP axis for different meshes

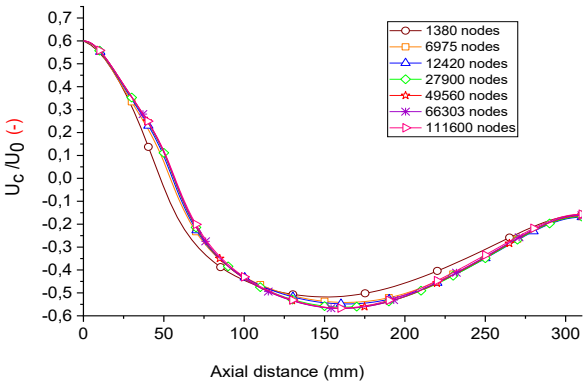

Fig.7 Velocity ratio profiles along the LSB3 CC axis for different meshes

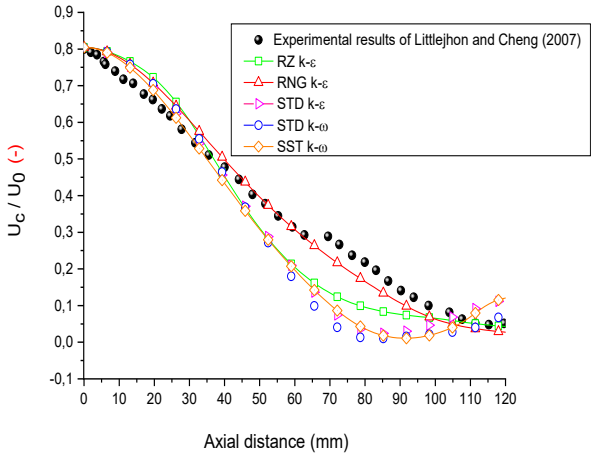

Fig. 8 Velocity ratio profiles on the LSB1 ATP burner axis

3. RESULTS AND DISCUSSION

Two combustion models (EDM and PPC) were combined with five different RANS turbulence models (STD k-ε, RNG k-ε, RZ k-ε, STD k-ω, and SST k-ω) to determine the most suitable turbulence and combustion model for LSB burners. CFD simulation results for various LSBs were compared to experimental data available in the literature.

3.1 Selection and Validation of Turbulence Model in Non-Reactive Flow

Figure 8 shows velocity **ratio** profiles in a low swirl atmospheric burner (LSB1 ATP) within non-reactive flow for distances ranging from 0 to 120 mm at r = 0, using various turbulence models.

It can be noted that the choice of turbulence model has a significant impact on simulation results. Compared to the experimental results, the RNG k-ε model accurately predicts the experimental velocity in the axial region. In contrast, the other turbulence models displayed discrepancies in axial velocity compared to the experimental results (Littlejohn & Cheng, 2007).

Furthermore, the findings show that all axial velocity values are positive, indicating the nonappearance of recirculation zones for non-reactive flow.

Two metrics were used to quantify the prediction model error. The first is the well-known and widely used RMSE (The Root Mean Squared Error), given by equation (28). The second metric, namely the dispersion coefficient, was used to obtain a relative value.

$$RMSE = \sqrt{\frac{\sum_{i=1}^{N}(V_{num}-V_{exp})^2}{N}} \quad (28)$$

Where: N is the number of experimental points, V_{exp} is the experimental value, and V_{num} is our simulation's calculated value.

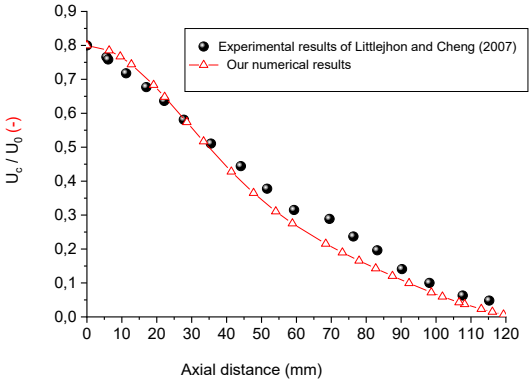

Fig. 9 Centerline velocity ratio profiles of the non-reactive flow

This confirmed that the RNG k-ε model reproduces accurately the results with a velocity dispersion coefficient of 3 %, compared to the experimental data.

3.2 Selection and Validation of Turbulence and Combustion Models in the Reactive Flow Case

This section aims to determine the most appropriate models for LSBs. Simulation results from five different turbulence models, combined first with the EDM combustion model, and then with the PPC model, are evaluated against experimental results with two types of burners. The first one is a low-swirl atmospheric burner, and the second is a burner in a combustion chamber. Temperature and velocity ratio profiles $\left(\frac{U_c}{U_0}\right)$ were used for this purpose.

3.2.1 Eddy Dissipation Combustion Model (EDM)

a. Case of low-swirl atmospheric burner

Figure 10 shows the evolution of the velocity in a low-swirl atmospheric burner (LSB1 ATP), and Fig.11 illustrates the evolution of temperature in a second low-swirl atmospheric burner (LSB2 ATP).

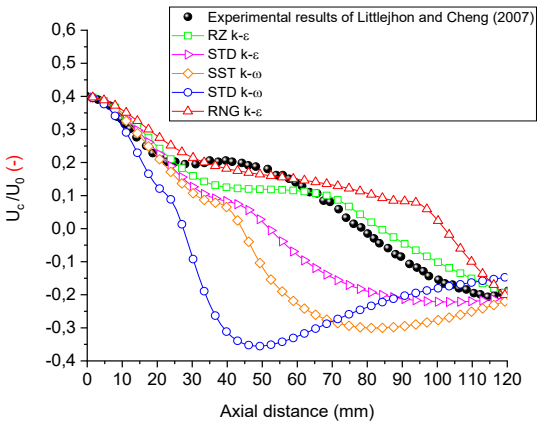

Fig. 10 Velocity ratio profiles along the LSB1 ATP axis for EDM

Table 6 RMSE and dispersion coefficient for EDM

Turbulence Model	EDM					
	LSB 1 ATP		LSB2 ATP		LSB3 CC	
	RMSE (-)	D (%)	RMSE (K)	D (%)	RMSE (-)	D(%)
STD k-ε	0.123	47.11	487.3	16.76	0.16	13.77
RNG k-ε	0.088	28.32	500.3	17.03	0.071	5.22
RZ k-ε	**0.042**	**9.68**	**276.1**	**7.92**	**0.05**	**4.44**
STD k-ω	0.268	67.21	757.8	31.74	0.308	24.42
SST k-ω	0.202	61.99	573.6	19.02	0.179	15.65

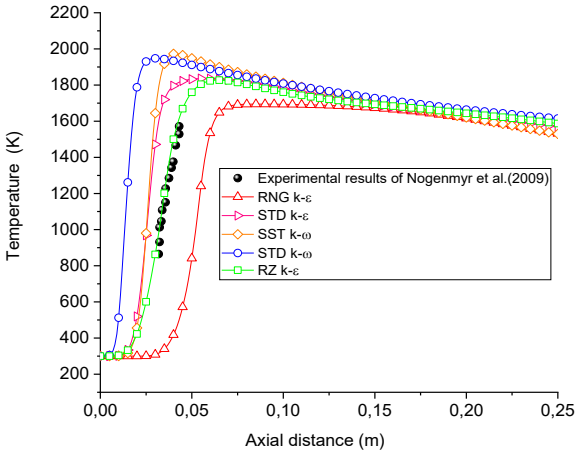

Fig. 11 Temperature profiles in the LSB2 ATP axis for EDM

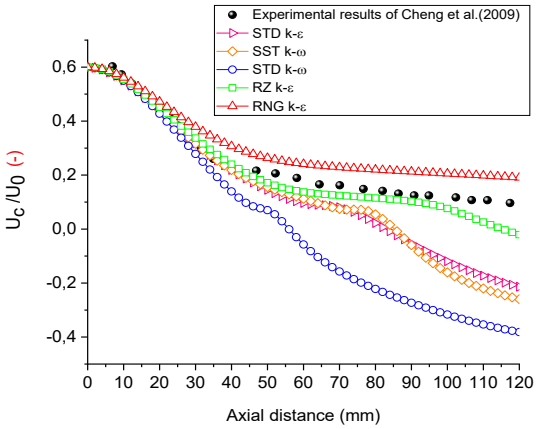

Fig. 12 Velocity ratio profiles in the LSB3 CC axis for EDM

b. Case of low-swirl burner in a combustion chamber

Figure 12 shows the evolution of the velocity of a low swirl burner in a combustion chamber (LSB3 CC) for the EDM combustion model coupled with five different turbulence models (STD k-ε, RNG k-ε, RZ k-ε, STD k-ω, and SST k-ω).

Figures 10, 11, and 12 show that the choice of the turbulence model to combine with the eddy dissipation combustion model significantly affects the simulation results. Compared to the experimental data (Littlejohn & Cheng, 2007; Cheng et al., 2009;), the RZ k-ε and RNG k-ε turbulence models provide better results than the other

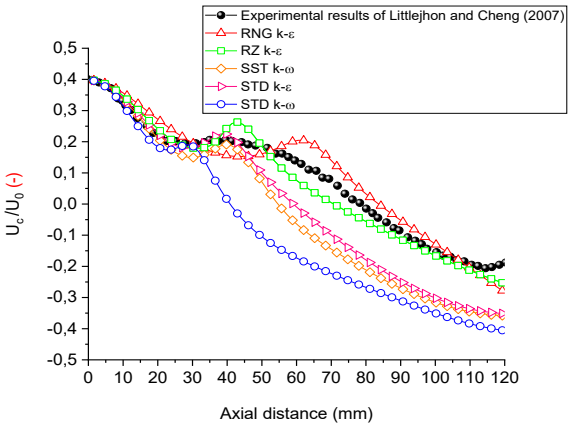

Fig. 13 velocity ratio profiles in the LSB1 ATP axis for PPC model

turbulence models. The velocity dispersion coefficient is 9.68% (Table 6 and Fig.16) for the LSB1 ATP scenario and 4.44% for the LSB3 CC scenario with the RZ k-ε model. However, in general, temperature is over-predicted when using EDM. The best results were obtained with the RZ k-ε turbulence model (Fig. 17).

It can be concluded that the RZ k-ε turbulence model is more suitable for the simulation of LSBs both under atmospheric and combustion chamber conditions when using the EDM combustion model. A similar conclusion was made by Cellek et al. (2023).

Table 6 summarizes RMSE and dispersion coefficient values for all the studied burners in the case of EDM. The optimal choice is highlighted.

3.2.2 Partially-Premixed Combustion (PPC) Model

a. Case of low swirl atmospheric burner

Figure 13 shows the evolution of the velocity for a low-swirl atmospheric burner (LSB1 ATP). Figure 14 illustrates temperature evolution in a second low-swirl atmospheric burner (LSB2 ATP). Simulation results from five different turbulence models coupled with the PPC model were compared with experimental results.

It is again shown (Figs. 13 and 14) that the choice of the turbulence model to combine with the partially premixed combustion model has an important effect on the simulation results. It can be observed that coupling the PPC model with the RNG k-ε turbulence model results in an interesting simulation prediction for the two burners. The corresponding velocity dispersion coefficient is

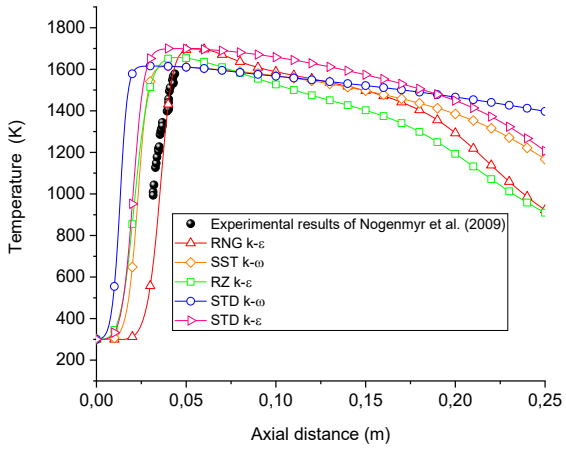

Fig. 14 Temperature profiles in the LSB2 ATP axis for the PPC model

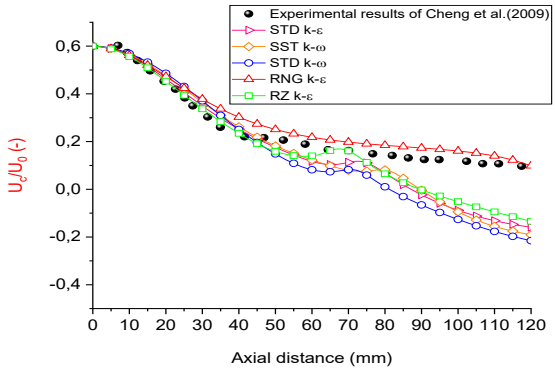

Fig. 15 Velocity ratio profiles in the LSB3 CC axis for the PPC model

11.66% (Table 7 and Fig.16) for LSB1 ATP and the lowest RMSE (Table 7 and Fig.17) for LSB2 ATP compared to experimental data (Littlejohn & Cheng, 2007; Nogenmyr et al., 2009), respectively. The RZ k-ε model achieved almost the same performance for LSB1 ATP (D =11.22%). Considering the two burners, k-ε RNG is the best choice.

b. Case of a low-swirl burner in a combustion chamber

Figure 15 shows the velocity evolution in the case of LSB in a combustion chamber (LSB3 CC) for the PPC model coupled with different turbulence models, compared to experimental data.

Figure 15 reveals that the choice of turbulence model has a considerable impact on the simulation results, especially from a certain axial distance. Compared to experimental data (Cheng et al., 2009), it can be seen that the RNG k-ε model combined with the PPC model provides better results than the other turbulence models, with a velocity dispersion coefficient of 2.22 % (Table 7). Thus, it appears that the RNG k-ε turbulence model is more convenient for the simulation of LSBs both under atmospheric and combustion chamber conditions when using the PPC model.

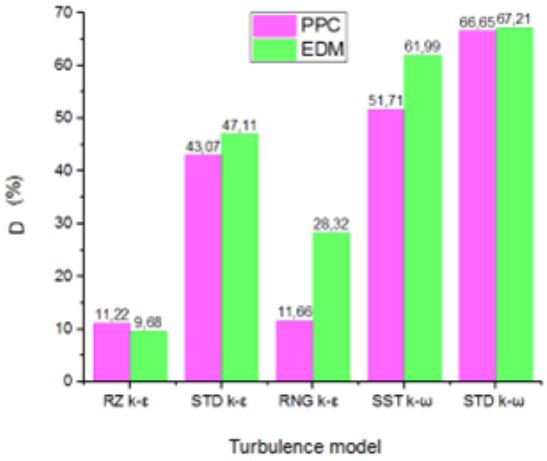

(a)

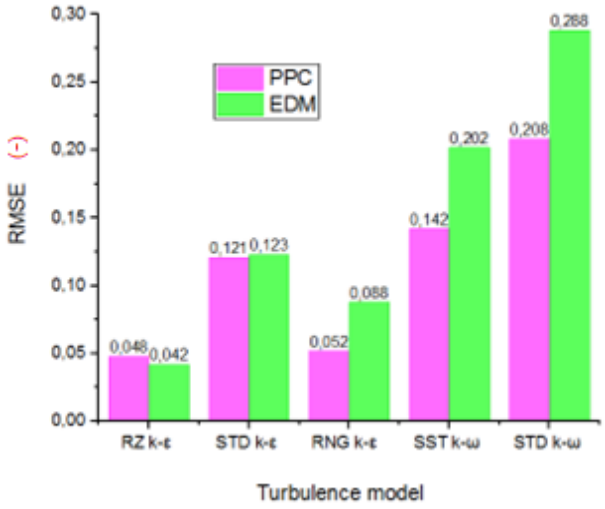

(b)

Fig. 16 (a) Dispersion coefficient (b) RMSE with PPC and EDM coupled to five turbulence models for LSB1 ATP

Figure 16 (a,b) shows comparisons of the dispersion coefficient and RMSE for the two combustion models (EDM and PPC) coupled with five turbulence models (STD k-ε, RNG k-ε, RZ k-ε, STD k-ω, and SST k-ω). Then, only RMSE is depicted.

Figures 17, and 18 show comparisons of RMSE for the two combustion models (EDM and PPC) coupled with five turbulence models (STD k-ε, RNG k-ε, RZ k-ε, STD k-ω, and SST k-ω) for two burners (LSB2 ATP and LSB3 CC).

It is clear from Figs. 16 (a,b),17, and 18 that considering the three burners, the RMSE is the lowest for the RNG k-ε coupled to the PPC model. However, the highest value was obtained for STD k-ω.

Table 7 summarizes RMSE and dispersion coefficient values for all the studied burners using the PPC model. The optimal choice is highlighted.

Table 7 RMSE and dispersion coefficient for PPC.

Turbulence Model	PPC Model					
	LSB 1 ATP		LSB2 ATP		LSB3 CC	
	RMSE (-)	D (%)	RMSE (K)	D (%)	RMSE (-)	D (%)
STD k-ε	0.121	43.07	524.7	21.61	0.132	11.4
RNG k-ε	**0.052**	**11.66**	**101.5**	**3.07**	**0.041**	**2.22**
RZ k-ε	**0.048**	**11.22**	456.7	16.90	0.114	9.98
STD k-ω	0.208	66.65	574.2	25.94	0.165	14.04
SST k-ω	0 .142	51.71	499.8	18.17	0.142	12.4

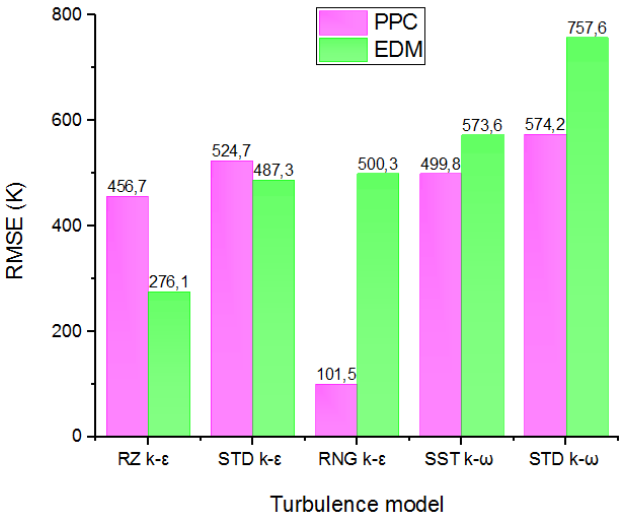

Fig. 17 RMSE with PPC and EDM coupled to five turbulence models for LSB2 ATP

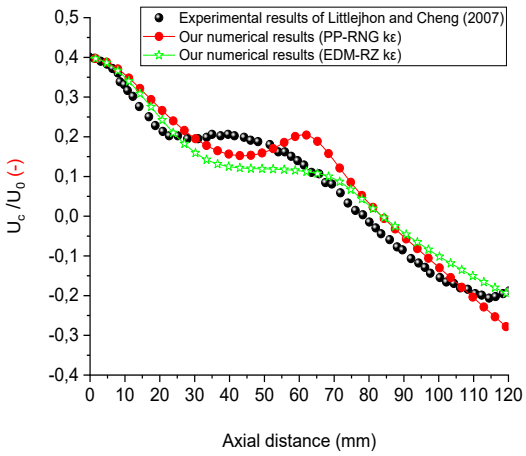

Fig. 19 Velocity ratio profiles along LSB1 ATP axis.

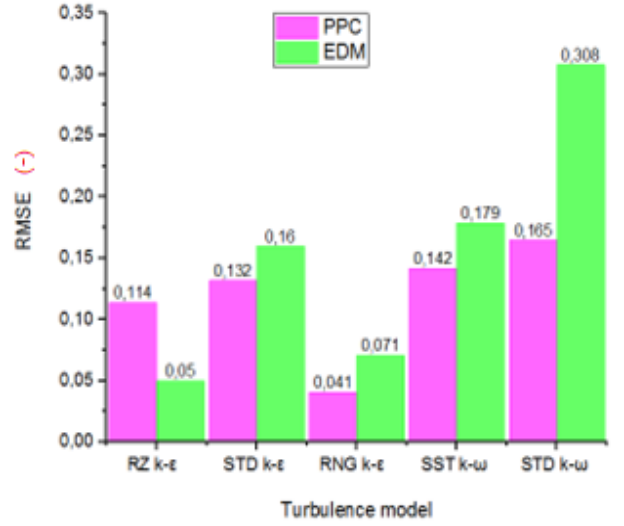

Fig. 18 RMSE with PPC and EDM coupled to five turbulence models for LSB3 CC

3.3 Comparative Study Between Partially-Premixed and Eddy Dissipation Combustion Models

From the above investigation, it is concluded that coupling the RZ k-ε turbulence model with the EDM combustion model is overall satisfactory for the simulation of LSBs both under atmospheric and combustion chamber conditions. In addition, the combination of the PPC model with the RNG k-ε turbulence model is interesting. It can be seen (Tables 6 and 7) that the error is within an acceptable interval. The maximum value of the dispersion coefficient is around 10%.

These two combinations are hereafter denoted as EDM-RZ kε and PP-RNG kε, respectively.

In the following section, a comparative study between those two combinations is carried out to determine the more pertinent choice.

3.3.1 Velocity and Temperature Profiles

Results concerning velocity and temperature profiles along the burner axis are presented in Figs. 19, 20, and 21.

Figure 19 depicts the axial velocity of the LSB1 ATP burner obtained using the EDM-RZ kε and PP-RNG kε models along with experimental data (Littlejohn & Cheng, 2007). Overall, the prediction of the two combinations is acceptable, even though the simulation results of EDM-RZ kε are slightly better. The velocity dispersion coefficient is 9.68% (Table 6 and Fig. 16) for the first combination and 11.66% (Table 7 and Fig. 16) for the second. It can be seen that the discrepancy compared to experimental results is mainly located at distances from x=30mm to 80mm.

In the case of LSB3 CC, simulation results concerning axial velocity obtained using PP-RNG kε models are very

Table 8 Computational time for different models' combinations

		Combustion models	
		PPC	**EDM**
Turbulence models	RNG k-ε	40min	1h27min
	RZ k-ε	37min	1h20min
	STD k-ε	32min	45min
	STD k-ω	42min	4h27min
	SST k-ω	24min	2h32min

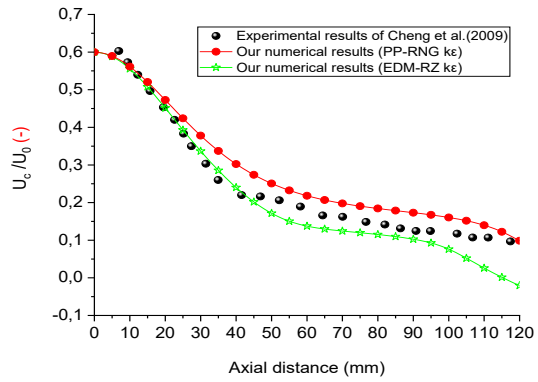

Fig. 20 Velocity ratio profiles along LSB3 CC axis

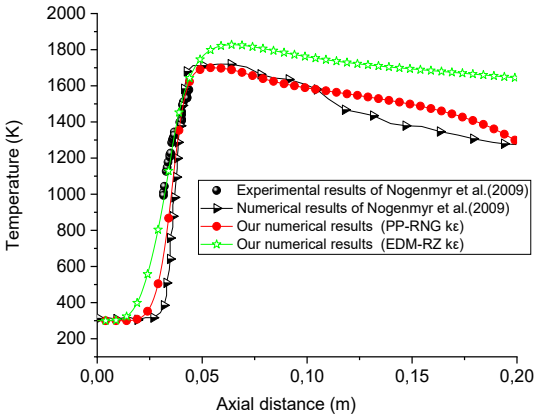

Fig. 21 Temperature profiles along LSB2 ATP axis

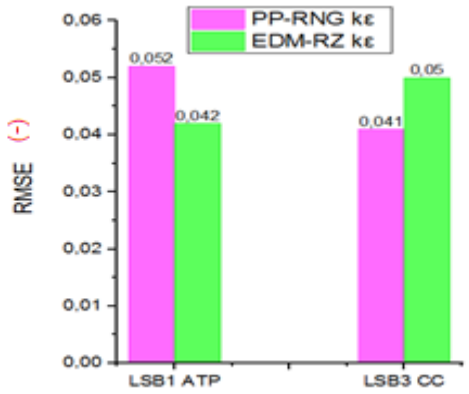

(a)

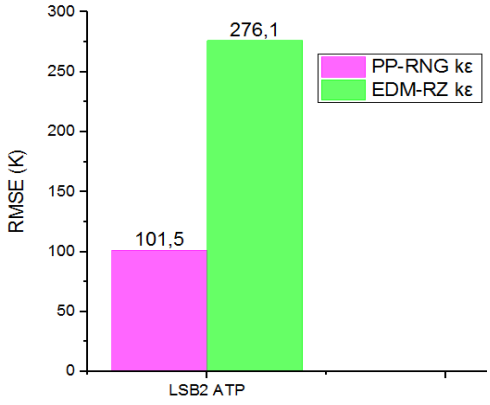

(b)

Fig. 22 RMSE for (EDM-kε RZ) and (PP-kε RNG) for (a) Velocity ratio for LSB1 3, and (b) Temperature for LSB2

satisfactory compared to experimental data (Cheng et al., 2009). The velocity dispersion coefficient is 2.22% (Table 7). Prediction using EDM-RZ kε models is also acceptable with a velocity dispersion coefficient of 4.44% (Table 6), even though a divergence from experimental data can be noticed from a certain distance.

Concerning temperature evolutions, profiles along the axis of the LSB2 ATP burner are shown in Fig. 21. Compared to experimental and numerical data (Nogenmyr et al., 2009), simulation results obtained with PP-RNG kε models are interesting. In addition, it can be seen that when the RNG k-ε turbulence model is coupled with the PPC model, the findings are very close to the LES simulation of the same reference for the entire axial distance. However, in general, temperature is over-predicted when using the EDM. The best results are obtained with the RZ k-ε turbulence model (Fig. 17).

In conclusion, considering the three burners, coupling the RNG k-ε turbulence model with the PPC model gives better simulation results than EDM-RZ kε models (Fig. 22).

The better performance of the PPC model over EDM can be explained by the fact that the PPC model is designed to handle situations where both premixed and non-premixed characteristics are present in the flow, as already mentioned. In LSBs, the fuel and oxidizer are often partially mixed. Thus, the PPC model matches this situation well. In addition, because LSBs are designed to maintain flame stability, and the PPC model can more

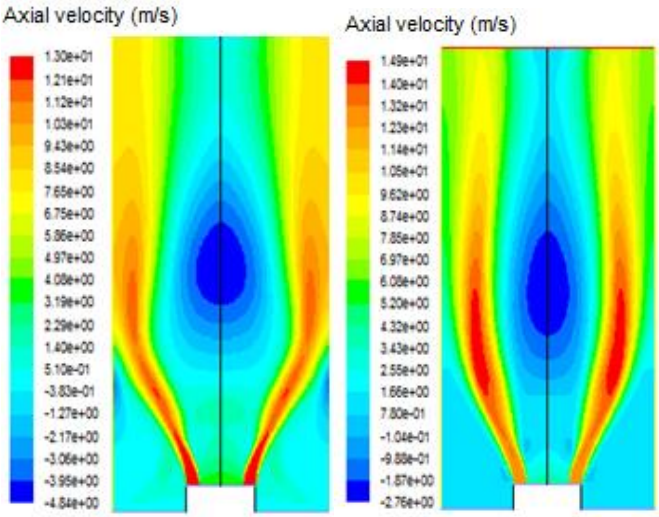

(a) EDM-RZ Kε (b) PP-RNG kε

Fig. 23 Axial velocity (m/s) contours for LSB1 ATP. (a) EDM-RZ kε , (b) PP-RNG kε.

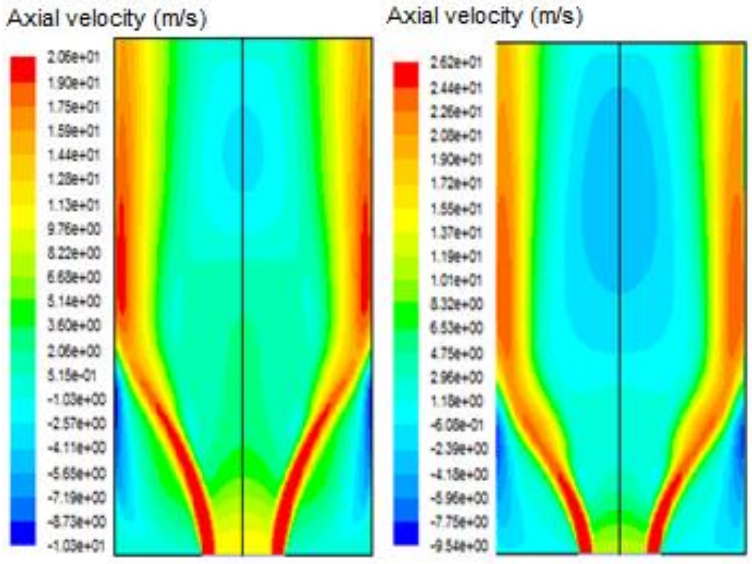

(a) EDM-RZ Kε (b) PP-RNG kε

Fig. 24 Axial velocity (m/s) contours for LSB3 CC. (a) EDM-RZ Kε , (b) PP-RNG kε.

accurately simulate the mixing and reaction rates under partially premixed cases, it allows for handling the stability and precise location of the flame front. Besides, the PPC model requires a source of ignition to initiate and trigger combustion, which is close to reality. On the other hand, the EDM does not require a source of ignition to initiate combustion, and remains limited by its reaction mechanism at one or two maximum stages. Moreover, the EDM assumes combustion is dominated by turbulence, which means it performs well in highly turbulent regimes. However, in low swirl burners, turbulence is generally low to moderate.

Furthermore, combining the PPC model with the RNG k-ε turbulence model, which is well suited for swirling flows, further improves its performance in this situation.

Concerning the computational time, Table 8 shows a summary for various models' combinations using a personal computer (Processor: Intel (R) Core (TM) i5-2450M CPU @2.50GHz, and 6 GB RAM).

It can be seen that when using the PPC model, the computational time did not exceed 42 min for all turbulence models. In the case of the EDM, the time is the longest when combined with k-ω models. It attained 4 h 27 min for STD k-ω.

Overall, this confirmed the low computational cost of the selected models.

3.3.2 Impact on Velocity and Temperature Contours

To see the impact of the model choice in detailed results, velocity and temperature contours obtained using the EDM-RZ kε and the PP-RNG kε models for LSB1 ATP, LSB3 CC, and LSB2 ATP were compared. Results are displayed in Figs. 23, 24, and 25.

Detailed results show that a considerable dissimilarity was found both qualitatively and quantitatively when

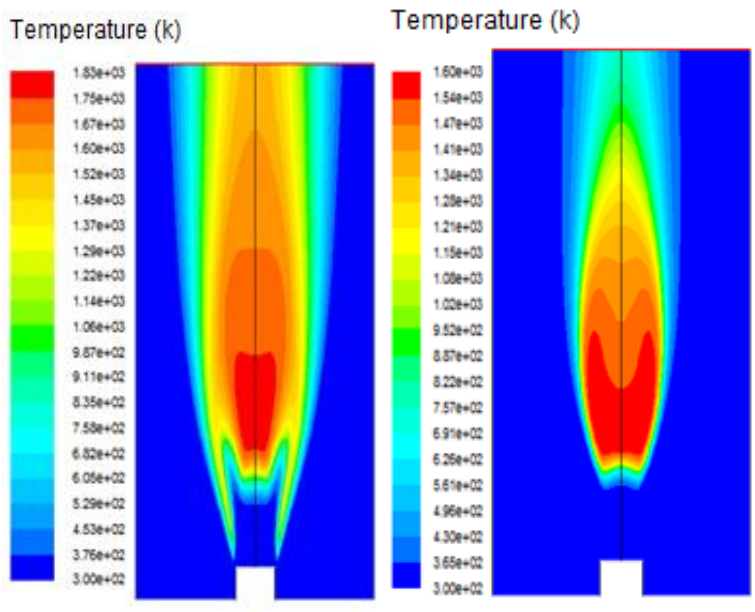

(a) EDM-RZ Kε (b) PP- RNG kε

Fig. 25 Temperature (K) contours for LSB2 ATP. (a) EDM-RZ Kε, (b) PP-RNG kε.

using the above-mentioned models. Flow, temperatures, and flame shape display differences.

The flame with EDM can reach higher velocity values than with the PPC model (Figs. 23 and 24). This can be justified by the infinitely fast chemistry of the EDM, which neglects the endothermic ignition reactions of CH_4 combustion. This neglect decreases the mixture density, which increases the velocity values in these zones. We can also see that recirculation zones are more important within EDM than for the PPC model

Figure 25 displays temperature contours, where it can be seen that the PPC model shows a different and shorter flame shape compared to the flame predicted by the EDM. Furthermore, the maximum temperature reached 1600K when coupling the RNG k-ε turbulence model with the PPC model, while it reached 1830K when using the RZ k-ε turbulence model with the EDM combustion model, confirming the over-prediction of temperatures.

Thus, coupling the RNG k-ε turbulence model with the PPC model is more pertinent for simulating reactive flow within LSBs under both atmospheric and combustion chamber conditions.

4. CONCLUSION

The present work aimed to determine the most suitable turbulence and combustion models for low-swirl burners simulations. Five turbulence models, namely the STD k-ε, RNG k-ε, RZ k-ε, STD k-ω, and SST k-ω, were examined. Two combustion models widely used in previously published works and less costly, were selected and investigated: the EDM and the PPC.

Simulation results were compared with experimental data from the literature. For more credibility of the outcomes, the investigation used experimental data of different LSB burners.

Analysis of the results allowed the following conclusions to be drawn:

-The influence of turbulence and combustion model choice is considerable.

-The k-ε STD and k-ω models are not a good choice for modeling swirl burners.

-Overall, the RZ k-ε and RNG k-ε turbulence models provide better results than other turbulence models.

- Coupling the RANS RNG k-ε turbulence model with the PPC model offers very satisfactory results.

-In general, temperature is overestimated when using the EDM. The best results are obtained with the RZ k-ε turbulence model.

-The better performance of the PPC model over the EDM can mainly be explained by the fact that the PPC model is designed to handle situations where both premixed and non-premixed characteristics are present in the flow. In LSBs, the fuel and oxidizer are often partially mixed. On the other hand, the EDM assumes combustion is dominated by turbulence, which means it performs well in highly turbulent regimes. However, in LSBs, turbulence is generally low to moderate. Moreover, the EDM remains limited by its reaction mechanism at one or two maximum stages.

-Because of the EDM limitations and outcomes, coupling the RNG k-ε turbulence model with the PPC model is more pertinent for simulating reactive flow within LSBs under both atmospheric and combustion chamber conditions. Therefore, it is our recommendation.

Future works: - As discussed in the assumptions in Section 2.1, it is still sufficient to limit the simulations to

axisymmetric 2D domains, thus saving significant amounts of computational time and effort. The present study and results of several investigations in the literature (Cellek & Pınarbaşı, 2018; Bouziane et al., 2021; Ouali et al., 2021; Xiao et al., 2022) confirmed the acceptability of this approach. However, a 3D simulation will allow assessing the improvement and the cost compared to the axisymmetric 2D approach.

- Results without radiation still give satisfactory agreement with experimental data (Bouziane et al.,2021; Ouali et al., 2021; Xiao et al., 2022). The present study results also validated this model. However, it is clear that including radiation effects will improve prediction accuracy. Thus, a comparison study is planned.

CONFLICT OF INTEREST

The authors declare that they have no known competing financial interests or personal relationships that could have appeared to influence the work reported in this paper.

AUTHOR CONTRIBUTIONS

Malika Ladjani: Conceptualization, Methodology, Writing-original draft. **Mohand Said Lounici:** Conceptualization, Methodology, Supervision, Writing-review and editing. **Sarah Ouchikh:** Methodology, Writing-review and editing.

REFERENCES

Abdulnaim, A., Elkholy, A., Elmously, M., Moneib, H., Roberts, W. L., & Elbaz, A. M. (2024). On the stability and characteristics of biogas/methane/air flames fired by a double swirl burner. *Flow, Turbulence and Combustion, 112*(3), 751-767. https://doi.org/10.1016/j.fuel.2022.123498

Al-Abdeli, Y. M., & Masri, A. R. (2015). Review of laboratory swirl burners and experiments for model validation. *Experimental Thermal and Fluid Science, 69*, 178-196. https://doi.org/10.1016/j.expthermflusci.2015.07.023

Anderson Jr, J. D. (1991). *Fundamentals of Aerodynamics, McGraw-Hill*.

Bedat, B., & Cheng, R. (1995). Experimental study of premixed flames in intense isotropic turbulence. *Combustion and Flame, 100*(3), 485-494. https://doi.org/10.1016/0010-2180(94)00138-I

Borghi, R., & Destriau, M. (1995). Combustion and Flames Edition Technip: Paris.

Bouziane, A., Alami, A., Zaitri, M., Bouchame, B., & Bouchetara, M. (2021). Investigation of swirl stabilized ch$_4$ air flame with varied hydrogen content by using computational fluid dynamics (CFD) to study the temperature field and flame shape. *Engineering, Technology & Applied Science Research, 11*(2), 6943-6948. https://doi.org/10.48084/etasr.4034

Carlsson, H., Carlsson, C., Fuchs, L., & Bai, X. S. (2014). Large eddy simulation and extended dynamic mode decomposition of flow-flame interaction in a lean premixed low swirl stabilized flame. *Flow, Turbulence and Combustion, 93*, 505-519. https://doi.org/10.1007/s10494-014-9560-6

Cellek, M. S., & Pınarbaşı, A. (2018). Investigations on performance and emission characteristics of an industrial low swirl burner while burning natural gas, methane, hydrogen-enriched natural gas and hydrogen as fuels. *International Journal of Hydrogen Energy, 43*(2), 1194-1207. https://doi.org/10.1016/j.ijhydene.2017.05.107.

Cellek, M. S., Pınarbaşı, A., Coskun, G., & Demir, U. (2023). The impact of turbulence and combustion models on flames and emissions in a low swirl burner. *Fuel, 343*, 127905. https://doi.org/10.1016/j.fuel.2023.127905

Chan, C., Lau, K., Chin, W., & Cheng, R. (1992). *Freely propagating open premixed turbulent flames stabilized by swirl.* Paper presented at the Symposium (International) on Combustion.

Cheng, R., Littlejohn, D., Strakey, P., & Sidwell, T. (2009). Laboratory investigations of a low-swirl injector with H2 and CH4 at gas turbine conditions. *Proceedings of the Combustion Institute, 32*(2), 3001-3009. https://doi.org/10.1016/j.proci.2008.06.141

Chong, C. T., Lam, S. S., & Hochgreb, S. (2016). Effect of mixture flow stratification on premixed flame structure and emissions under counter-rotating swirl burner configuration. *Applied Thermal Engineering, 105*, 905-912. https://doi.org/10.1016/j.applthermaleng.2016.03.164

Daurer, G., Schwarz, S., Demuth, M., Gaber, C., & Hochenauer, C. (2024). Experimental and numerical analysis of industrial-type low-swirl combustion of hydrogen enriched natural gas including OH* chemiluminescence imaging. *International Journal of Hydrogen Energy, 80*, 890-906. https://doi.org/10.1016/j.ijhydene.2024.07.119

Fluent, A. (2015). *Theory guide: ANSYS Canonsburg*.

Fudihara, T., Goldstein Jr, L., & Mori, M. (2003). The three-dimensional numerical aerodynamics of a movable block burner. *Brazilian Journal of Chemical Engineering, 20*, 391-401. https://doi.org/10.1590/S0104663220030004000006

Gong, Y., Fredrich, D., Marquis, A. J., & Jones, W. P. (2023). Numerical investigation of combustion instabilities in swirling flames with hydrogen enrichment. *Flow, Turbulence and Combustion, 111*(3), 953-993. https://doi.org/10.1007/s10494-023-00476-5

Li, X., & Jia, L. (2014). Investigation on combustion characteristics and NO formation of methane with swirling and non-swirling high temperature air. *Journal of Thermal Science, 23*, 472-479. https://doi.org/10.1007/s11630-014-0731-5

Littlejohn, D., & Cheng, R. (2007). Fuel effects on a low-swirl injector for lean premixed gas turbines. *Proceedings of the Combustion Institute, 31*(2), 3155-3162. https://doi.org/10.1016/j.proci.2006.07.146

Magnussen, B. F., & Hjertager, B. H. (1977). *On mathematical modeling of turbulent combustion with special emphasis on soot formation and combustion.* Paper presented at the Symposium (international) on Combustion.

Mazzotta, L., Lamioni, R., Agati, G., Evangelisti, A., Rispoli, F., Valera-Medina, A., & Borello, D. (2025). On the impact of CFD turbulence models for premixed NH_3/H_2 combustion on emissions and flame characteristics in a swirl-stabilized burner. *Flow, Turbulence and Combustion*, 1-21 https://doi.org/10.1007/s10494-025-00638-7

Muppala, S., Manickam, B., & Dinkelacker, F. (2015). A comparative study of different reaction models for turbulent methane/hydrogen/air combustion. *Journal of Thermal Engineering, 1*(5), 367-380. https://doi.org/10.18186/jte.60394

Nanduri, J., Parsons, D. R., Yilmaz, S. L., Celik, I. B., & Strakey, P. A. (2010). Assessment of RANS-based turbulent combustion models for prediction of emissions from lean premixed combustion of methane. *Combustion Science and Technology, 182*(7), 794-821. https://doi.org/10.1080/00102200903341546

Nemitallah, M. A., Aljehani, S. K., & Haque, M. A. (2023). Effects of fuel-hydrogen levels on combustion, operability, and emission parameters of CH4/H2/O2/CO2 stratified flames in a dual-swirl gas turbine burner. *Engineering Applications of Computational Fluid Mechanics, 17*(1), 2229406.

Nogenmyr, K. J., Fureby, C., Bai, X. S., Petersson, P., Collin, R., & Linne, M. (2009). Large eddy simulation and laser diagnostic studies on a low swirl stratified premixed flame. *Combustion and Flame, 156*(1), 25-36. https://doi.org/10.1016/j.combustflame.2008.06.014

Ouali, S., Bentebbiche, A., & Belmrabet, T. (2016). Numerical simulation of swirl and methane equivalence ratio effects on premixed turbulent flames and NOx apparitions. *Journal of Applied Fluid Mechanics, 9*(2), 987-998. https://doi.org/10.18869/acadpub.jafm.68.225.22603

Pang, Y. S., Law, W. P., Pung, K. Q., & Gimbun, J. (2018). A Computational Fluid Dynamics Study of Turbulence, Radiation, and Combustion Models for Natural Gas Combustion Burner. *Bulletin of Chemical Reaction Engineering & Catalysis, 13*(1), 155-169. https://doi.org/10.9767/bcrec.13.1.1395.155-169

Pashchenko, D. (2020). Hydrogen-rich fuel combustion in a swirling flame: CFD-modeling with experimental verification. *International Journal of Hydrogen Energy, 45*(38), 19996-20003. https://doi.org/10.1016/j.ijhydene.2020.05.113.

Rahman, T. M. R., Asrar, W., & Khan, S. A. (2019). An investigation of RANS simulations for swirl-stabilized isothermal turbulent flow in a gas turbine burner. *CFD Letters, 11*(9), 14–31. https://akademiabaru.com/submit/index.php/cfdl/article/view/3181

Stefanizzi, M., Stefanizzi, S., Ceglie, V., Capurso, T., Torresi, M., & Camporeale, S. M. (2021). *Analysis of the partially premixed combustion in a labscale swirl-stabilized burner fueled by a methane-hydrogen mixture.* Paper presented at the E3S Web of Conferences. https://doi.org/10.1051/e3sconf/202131211004

Tidswell, M., Muppala, S., & Rao, V. C. M. (2018). *A numerical study of two turbulent flame speed models for H_2/CH_4/air premixed combustion.* Paper presented at the International Conference on Combustion Physics and Chemistry.

Xiao, C., Omidi, M., Surendar, A., Alizadeh, A. A., Bokov, D. O., Binyamin, & Toghraie, D. (2022). Simulation of combustion flow of methane gas in a premixed low-swirl burner using a partially premixed combustion model. *Journal of Thermal Science, 31*(5), 1663-1681. https://doi.org/10.1007/s11630-022-1611-z